Human Molecular Genetics, 2009, Vol. 18, No. 11 **1909–1923**
doi:10.1093/hmg/ddp112
Advance Access published on March 11, 2009

Defects in neural stem cell proliferation and olfaction in *Chd7* deficient mice indicate a mechanism for hyposmia in human CHARGE syndrome

W.S. Layman[1], D.P. McEwen[2], L.A. Beyer[3], S.R. Lalani[5], S.D. Fernbach[5], E. Oh[6], A. Swaroop[6], C.C. Hegg[7], Y. Raphael[3], J.R. Martens[2] and D.M. Martin[1,4,*]

[1]Department of Human Genetics, [2]Department of Pharmacology, [3]Department of Otolarynology and [4]Department of Pediatrics, University of Michigan Medical Center, 3520A Medical Science Research Building I, Ann Arbor, MI 48109-5652, USA, [5]Department of Molecular and Human Genetics, Baylor College of Medicine, Houston, TX 77030, USA, [6]Neurobiology Neurodegeneration and Repair Laboratory (N-NRL), National Eye Institute / NIH, Bethesda, MD 20892, USA and [7]Department of Pharmacology and Toxicology, Michigan State University, East Lansing, MI 48824, USA

Received December 5, 2008; Revised March 2, 2009; Accepted March 9, 2009

Mutations in *CHD7*, a chromodomain gene, are present in a majority of individuals with CHARGE syndrome, a multiple anomaly disorder characterized by ocular Coloboma, Heart defects, Atresia of the choanae, Retarded growth and development, Genital hypoplasia and Ear anomalies. The clinical features of CHARGE syndrome are highly variable and incompletely penetrant. Olfactory dysfunction is a common feature in CHARGE syndrome and has been potentially linked to primary olfactory bulb defects, but no data confirming this mechanistic link have been reported. On the basis of these observations, we hypothesized that loss of *Chd7* disrupts mammalian olfactory tissue development and function. We found severe defects in olfaction in individuals with *CHD7* mutations and CHARGE, and loss of odor evoked electro-olfactogram responses in *Chd7* deficient mice, suggesting reduced olfaction is due to a dysfunctional olfactory epithelium. *Chd7* expression was high in basal olfactory epithelial neural stem cells and down-regulated in mature olfactory sensory neurons. We observed smaller olfactory bulbs, reduced olfactory sensory neurons, and disorganized epithelial ultrastructure in *Chd7* mutant mice, despite apparently normal functional cilia and sustentacular cells. Significant reductions in the proliferation of neural stem cells and regeneration of olfactory sensory neurons in the mature *Chd7*$^{Gt/+}$ olfactory epithelium indicate critical roles for *Chd7* in regulating neurogenesis. These studies provide evidence that mammalian olfactory dysfunction due to *Chd7* haploinsufficiency is linked to primary defects in olfactory neural stem cell proliferation and may influence olfactory bulb development.

INTRODUCTION

CHD7 haploinsufficiency in humans causes CHARGE syndrome, a clinically variable, multiple anomaly condition with an estimated incidence of 1:8500–1:12000 (1–3). CHARGE is characterized by ocular Coloboma, Heart defects, Atresia of the choanae, Retarded growth and development, Genital hypoplasia and Ear abnormalities including deafness and vestibular disorders (4). CHARGE individuals also have variably penetrant craniofacial abnormalities, hypogonadotropic hypogonadism and olfactory dysfunction (4–11). Heterozygosity for nonsense, deletion or missense *CHD7* mutations is estimated to occur in 60–80% of patients with CHARGE syndrome; these mutations are distributed throughout the coding sequence and do not appear to be correlated with specific aspects of the clinical phenotype

*To whom correspondence should be addressed. Tel: +1 7346474859; Fax: +1 7347639512; Email: donnamm@umich.edu

(5–11). Most human *CHD7* mutations identified thus far are *de novo*; however, evidence for germline mosaicism has been suggested for families with multiple affected siblings (6,12–14). Magnetic resonance imaging shows olfactory bulb defects ranging from hypoplasia to complete absence in all CHARGE individuals tested and olfactory dysfunction in a majority of patients (15–20).

Chd7 is widely expressed during murine and human embryonic development, and in many neural tissues including forebrain, midbrain, hindbrain, optic nerve, retina, trigeminal ganglion, facial ganglion, glossopharyngeal ganglion, dorsal root ganglion and enteric neurons (8,21,22). *Chd7* is also expressed in developing human and mouse olfactory bulb and olfactory epithelium (8,21,22), suggesting a role for CHD7 in olfaction. The olfactory system provides a unique model in which to analyze the role of CHD7 in neuronal development, due to the rapid turnover of the olfactory epithelium with continuous neurogenesis of olfactory sensory neurons during development and into adulthood. A better understanding of the mechanisms underlying olfaction and neuronal regeneration in adult tissues could give insights into therapies directed toward neural regeneration, and elucidate the role of CHD7 in olfactory development and maintenance.

CHD7 is one of nine members of a family of chromatin remodeling proteins that are characterized by the presence of two chromodomains, a centrally located helicase domain and less well-defined carboxyl terminal domains (23,24). These nine CHD proteins are subdivided into three classes based upon their amino acid sequence and functional protein domains (25–29). CHD proteins use ATP hydrolysis to regulate access to DNA by altering nucleosome structure (25–29). There is also evidence that CHD7 may regulate transcription elongation. The *CHD7 Drosophila* ortholog *Kismet* down-regulates transcriptional elongation by RNA polymerase II through the recruitment of ASH1 and TRX and may be involved in the maintenance of stem cell pluripotency by regulating methylation of histone H3 lysine 27 (30). CHD7 is also implicated in cell fate specification of mesenchymal stem cells (31). During osteoblast and adipocyte differentiation, CHD7 forms a complex with NLK, SETDB1 and PPAR-γ, then binds to methylated lysine 4 and lysine 9 residues on histone H3 at PPAR-γ target promoters and suppresses ligand-induced transactivation of PPAR-γ target genes which leads to a change in cell fate (31). Together, these data suggest that CHD7 regulates gene transcription with effects on stem cell differentiation.

Here, we show that CHARGE individuals with mutations in *CHD7* have variably impaired olfaction, and *Chd7* deficient mice also have severely impaired olfaction with hypoplastic olfactory bulbs. We found high *Chd7* expression in adult mouse olfactory epithelial stem cells including proliferating basal cells and pro-neuronal basal cells, but reduced *Chd7* expression in the adult olfactory bulb. *Chd7* deficient mice have a significant decrease in olfactory neural stem cell proliferation, leading to a reduction in olfactory sensory neurons. These data help to clarify the structural impact of *Chd7* deficiency on olfactory neuronal production and regeneration, and implicate a role for CHD7 in neural stem cell differentiation.

Table 1. B-SIT olfactory function scores for CHARGE individuals

Patient no.	B-SIT score	Exon	Mutation	*De novo* versus familial
1	3	2	R312X	Unknown
2	1	11	c.2836-15C>G	Unknown
3	5	12	L1007P3	Unknown
4	0	12	T1027_P1029del	*De novo*
5	1	20	R1557fsX1558	Unknown
6	8	33	R2319S	Familial
7	9	33	R2319S	Familial
8	11	33	W2332X	*De novo*

Humans with *CHD7* mutations and CHARGE syndrome have variable reductions in olfaction. Brief Smell Identification Tests (B-SIT) were performed on eight individuals with *CHD7* mutations and a clinical phenotype of CHARGE. B-SIT scores of 9 or higher are considered normal.

RESULTS

Olfaction is reduced in human CHARGE patients and in mice with *Chd7* deficiency

Olfactory defects and olfactory bulb hypoplasia have previously been reported in CHARGE individuals (15–20,32). However, there is minimal information about olfactory status in individuals with CHARGE phenotypes and documented *CHD7* mutations. We analyzed eight individuals with CHARGE (and confirmed mutations in *CHD7)* (7) for defects in olfaction, using the Brief Smell Identification Test (B-SIT) (Table 1). B-SIT is a self-administered, scratch and sniff test booklet that measures whether an individual can accurately identify 12 different odorants. It is important to note that random guessing would result in a score of 3. We found that six of eight individuals with CHARGE aged 10 years or older had B-SIT scores of 8 or lower, whereas a score of 9–12 is considered to reflect normal olfactory function. The 8 scores from individuals with CHARGE ranged from 0 to 11, and included misidentification of all odorants represented in the test. Interestingly, individuals 6, 7 and 8 all did well on the B-SIT test, with scores of 8 or higher. These individuals all have mutations in exon 33 (individuals 6 and 7 have missense mutations, whereas individual 8 has a nonsense truncating mutation). Exon 33 is a 3' exon that does not encode any of the well-characterized protein domains in CHD7 (chromodomain, helicase, SNF2, BRK or SANT). Further analyses are needed to determine whether olfactory ability correlates with specific *CHD7* genotypes, and whether certain CHD7 protein domains are more important than others for olfactory function.

On the basis of the high prevalence of olfactory defects in individuals with CHARGE, we hypothesized that similar defects might be present in *Chd7* deficient mice. To test this hypothesis, we used $Chd7^{Gt/+}$ mice that are heterozygous for a gene trapped *lacZ* allele (22). Homozygous $Chd7^{Gt/Gt}$ mice are embryonic lethal after E10.5, presumably from cardiac or other internal organ defects (21,22). To test for olfactory function in $Chd7^{Gt/+}$ mice, we analyzed 6-week-old wild-type ($n = 8$) and $Chd7^{Gt/+}$ ($n = 7$) sex-matched littermate mice by electro-olfactogram (Fig. 1). Mice were tested with amyl

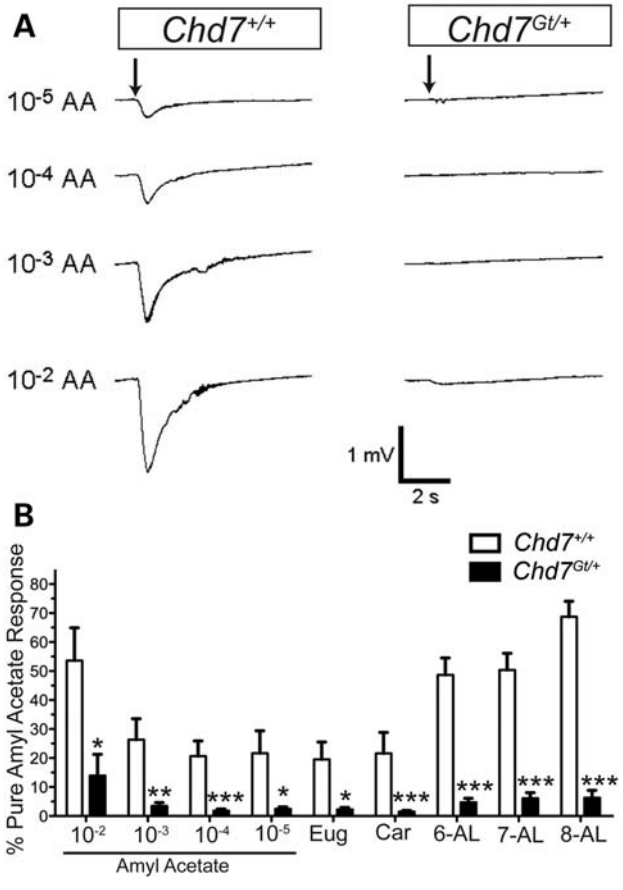

Figure 1. $Chd7^{Gt/+}$ mice have severely impaired olfaction. (**A**) Electro-olfactogram tracings from adult wild-type and $Chd7^{Gt/+}$ mice. The olfactory epithelium from each mouse was exposed to four different concentrations of amyl acetate. (**B**) Histogram of electro-olfactogram responses from wild-type (open bars; $n = 8$) and $Chd7^{Gt/+}$ (solid bars; $n = 7$) mice shows four different concentrations of amyl acetate and five additional odorants tested at 10^{-3} M. Each response was normalized and expressed as a percentage of a pure amyl acetate pulse given during the same trace. AA, amyl acetate; 8-AL, octanal; 7-AL, haptaldehyde; 6-AL, hexanal; Eug, eugenol; Car, carvone. $^{*}P < 0.05$, $^{**}P < 0.005$ and $^{***}P < 0.001$ as determined by unpaired Student's *t*-test.

acetate at four different concentrations (Fig. 1A), as well as five additional odorants (octanal, haptaldehyde, hexanal, eugenol and carvone) at 10^{-3} M (Fig. 1B). $Chd7^{Gt/+}$ mice had little to no response to any odorant at the concentrations tested by electro-olfactogram (Fig. 1). These data provide definitive evidence that $Chd7^{Gt/+}$ mice have severely impaired olfactory function compared with wild-type littermates, for all odorants tested and they demonstrate for the first time that this impairment occurs at the level of the olfactory epithelium.

Chd7 is expressed in developing and mature olfactory epithelium

Chd7 mRNA is expressed in developing mouse olfactory tissues (21,22). To localize CHD7 protein in the olfactory system, we used two independent approaches. We used $Chd7^{Gt/+}$ mice that express β-galactosidase from the *Chd7* locus (22) and compared β-galactosidase expression with immunofluorescence for CHD7 using anti-CHD7 antibody (Fig. 2). We detected high β-galactosidase activity (Fig. 2A and B) and anti-CHD7 immunofluorescence (Fig. 2C–F) in the developing olfactory epithelium and olfactory bulb. There was a slight reduction in anti-CHD7 immunofluorescence in the olfactory epithelium of $Chd7^{Gt/+}$ embryos compared with wild-type littermates (Fig. 2C and D), consistent with *Chd7* haploinsufficiency at the $Chd7^{Gt}$ allele.

To test whether *Chd7* expression continues into adulthood in mouse olfactory tissues, we performed antibody staining with anti-CHD7 on the 6-week-old adult mouse olfactory epithelium and olfactory bulb. We found that *Chd7* is highly expressed in the mature olfactory epithelium (Fig. 2G–L) and is weakly expressed in the adult olfactory bulb (Supplementary Material, Fig. S1). We also found CHD7 expression in the adult mouse rostral migratory stream (Supplementary Material, Fig. S1). These observations are consistent with adult brain *Chd7* mRNA expression patterns [available online at the Allen Brain Atlas (http://www.brain-map.org/)]. We observed some regional differences in the distribution of CHD7-positive cells in both the wild-type and the $Chd7^{Gt/+}$ olfactory epithelium (Fig. 2G and H). In wild-type mice, a majority of the olfactory epithelium contained CHD7-positive cells in the basal portion of the epithelium with a small proportion of CHD7-positive cells residing in the apical portion. $Chd7^{Gt/+}$ mice appeared to have fewer CHD7-positive cells in the olfactory epithelium, most of which resided in the basal portion of the epithelium (Fig. 2G and H). Olfactory epithelial crypts (recessed regions) in both wild-type and $Chd7^{Gt/+}$ mice had CHD7-positive cell nuclei occupying the basal, medial and apical portions of the epithelium (Fig. 2K and L). These data indicate that *Chd7* expression is regionally distributed throughout the adult olfactory epithelium of both wild-type and $Chd7^{Gt/+}$ mice.

Chd7 is expressed in olfactory neural stem cells

The olfactory epithelium contains a variety of well defined, functionally and structurally distinct cell types (33). In order to identify CHD7-positive cell types within the adult olfactory epithelium, we used immunofluorescence with anti-CHD7 and cell type-specific antibodies. Olfactory marker protein (OMP) labels mature olfactory sensory neurons in the postnatal olfactory epithelium (33,34). We found that most CHD7-positive cells in the olfactory epithelium were OMP-negative in both wild-type and $Chd7^{Gt/+}$ mice (Fig. 3A and B). However, the distribution and intensity of OMP immunofluorescence in $Chd7^{Gt/+}$ olfactory epithelium was altered compared with wild-type littermates (Fig. 3B). There was 16% less anti-OMP immunofluorescence of mature olfactory sensory neurons measured by ImageJ software in the $Chd7^{Gt/+}$ olfactory epithelium, and this OMP label appeared disorganized compared with wild-type (Fig. 3B). These data are consistent with an abnormality in olfactory sensory neurons in $Chd7^{Gt/+}$ mice.

Since a majority of CHD7-positive cells are located in the basal portion of the epithelium (Fig. 2I and J), it was important to distinguish which population of basal cells were CHD7-positive. To characterize the CHD7-positive basal cells in the mature olfactory epithelium, we used antibodies

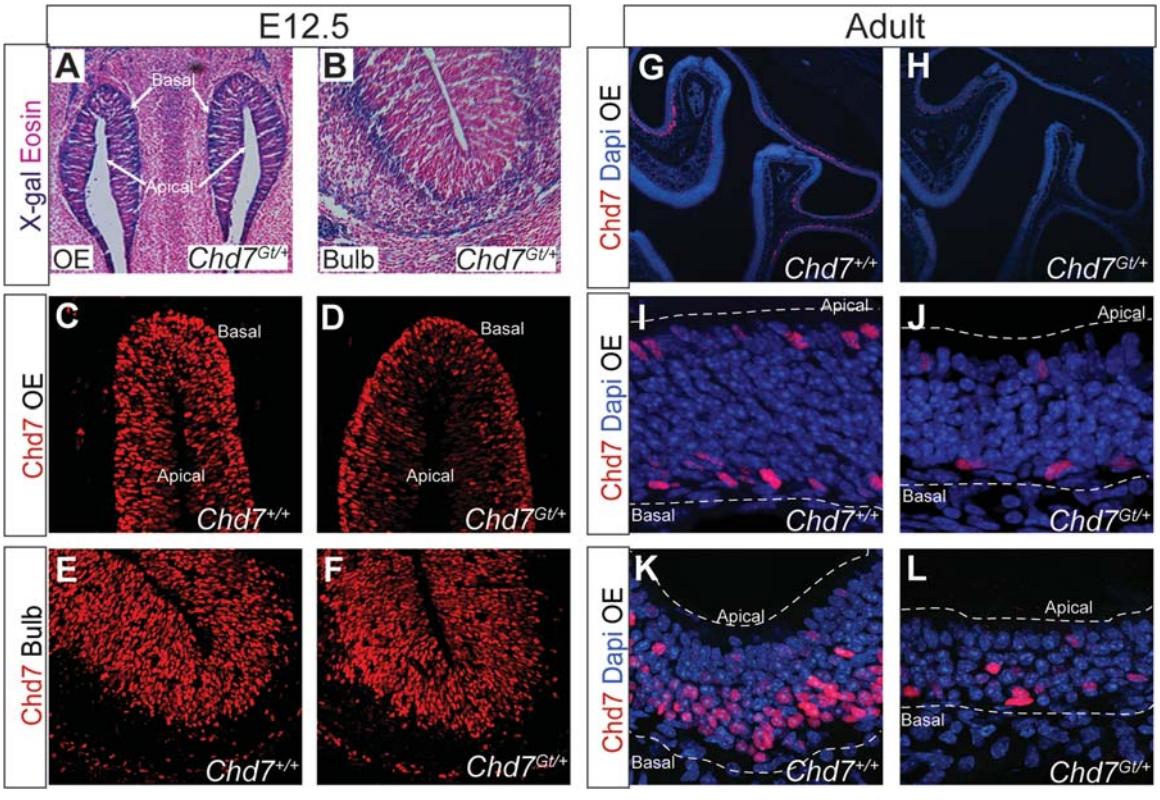

Figure 2. *Chd7* is expressed in developing and mature olfactory tissues. X-gal staining shows *Chd7* expression in the embryonic olfactory epithelium (**A**) and bulb (**B**). Immunofluorescence with anti-CHD7 shows *Chd7* expression in embryonic E12.5 olfactory epithelium (**C** and **D**) and bulb (**E** and **F**) and in the adult olfactory epithelium (**G**–**L**). *Chd7* expression in the adult olfactory epithelium is regionally variable (G and H), with most CHD7-positive cells present in the basal and apical regions of the olfactory epithelium (I and J). A few regions of the olfactory epithelium contain CHD7-postive cells which span the olfactory epithelium (basal to apical), typically in crypt regions where the epithelium undergoes acute turns in orientation (K and L). White dotted lines in (I–L) indicate apical and basal surfaces of the epithelium.

against Mash1 and NeuroD, markers of early (Mash1) and late (NeuroD) pro-neuronal basal stem cells. Mash1 is a basic helix–loop–helix (bHLH) transcription factor thought to be a pro-neuronal determination gene that initiates neuronal differentiation (33). NeuroD is a bHLH transcription factor whose expression is thought to drive cell cycle exit and determination of neuronal cell fate (33). We detected co-localization of CHD7 with Mash1 (Fig. 3C and D) and NeuroD (Fig. 3E and F) in basal cells of wild-type and *Chd7*$^{Gt/+}$ olfactory epithelium. These observations provide evidence that *Chd7* is expressed in pro-neuronal basal cells of the adult olfactory epithelium, in both wild-type and *Chd7*$^{Gt/+}$ mice.

Sustentacular cells and microvillar cells are the two known cell types located in the apical portion of the olfactory epithelium. Sustentacular cells comprise the majority of apical cells and are thought to represent a glial-like population of cells. To test whether CHD7-positive cells in the apical portion of the epithelium represented sustentacular cells, we used an antibody against receptor expression-enhancing protein 6 (Reep6) (35). We found colocalization between CHD7 and REEP6 in both wild-type and *Chd7*$^{Gt/+}$ olfactory epithelium (Fig. 3G and H). We also found colocalization of CHD7 and Sus1, another marker of sustentacular cells (Fig. 3I and J). In addition, anti-Sus1 appeared to label a subset of microvillar cells, based upon cellular morphology. CHD7 colocalized with Sus1 in some of these microvillar appearing cells (arrow, Fig. 3I). These data indicate that *Chd7* is expressed in sustentacular cells and perhaps also in some microvillar cells of the olfactory epithelium.

Olfactory bulb neuronal defects in *Chd7*$^{Gt/+}$ mice

Clinical data in humans with CHARGE have suggested a high prevalence of olfactory bulb defects, ranging from complete absence of the bulbs to mild hypoplasia or asymmetry (15–20). We found statistically significant differences in brain, telencephalon and olfactory bulb length between adult wild-type and *Chd7*$^{Gt/+}$ mutant mice (Fig. 4A, B, I and J). There were no differences in olfactory bulb width (Fig. 4A, B, I and J) or morphology, based on H&E staining of wild-type and *Chd7*$^{Gt/+}$ mutant mice (Fig. 4C, D and I). Olfactory bulb hypoplasia in *Chd7*$^{Gt/+}$ mice is consistent with olfactory bulb defects found in CHARGE individuals. However, *Chd7*$^{Gt/+}$ mice may also have a subtle abnormality in olfactory bulb neuronal architecture or function. To test this, we used anti-OMP that marks olfactory sensory neuron projections in the olfactory bulb glomeruli. We found intact OMP-positive glomeruli in both wild-type and *Chd7*$^{Gt/+}$ olfactory bulb (Fig. 4E and F), arguing against a major defect in olfactory sensory neuronal architecture. To further analyze olfactory sensory neuron activity, we labeled dopaminergic interneurons

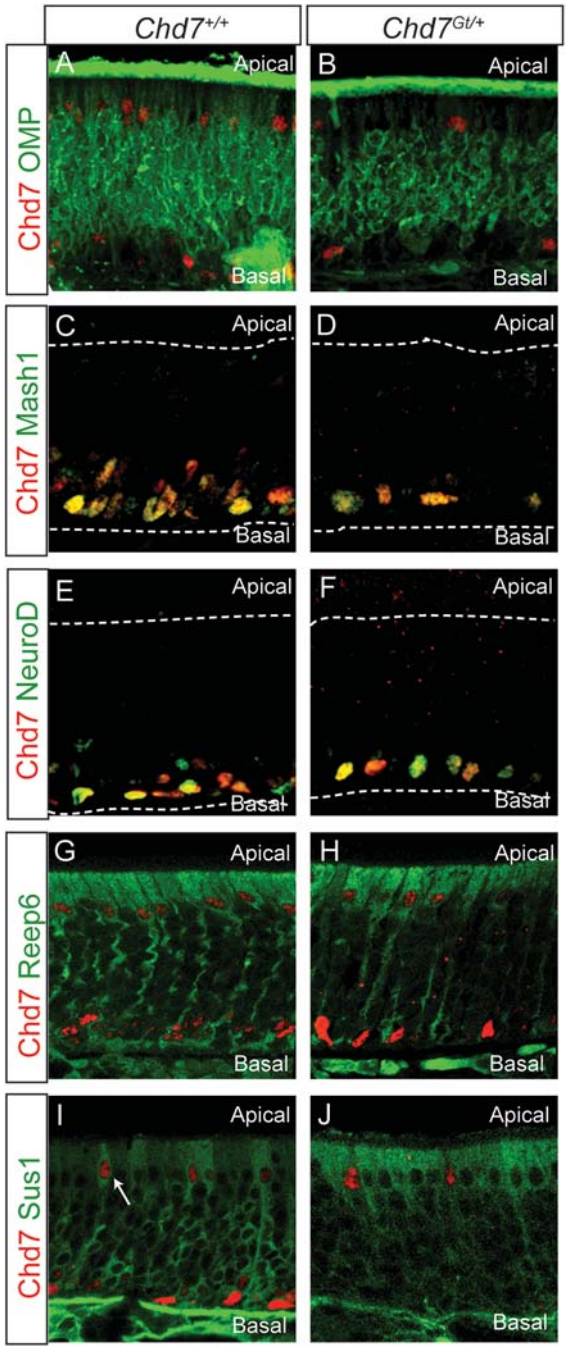

Figure 3. *Chd7* is expressed in basal stem cells in the mature olfactory epithelium. The adult olfactory epithelium from wild-type and $Chd7^{Gt/+}$ mice is stained with anti-CHD7 and antibodies against OMP (**A** and **B**), Mash1 (**C** and **D**), NeuroD (**E** and **F**), Reep6 (**G** and **H**) and Sus1 (**I** and **J**). CHD7-positive cells in the apical and basal domains do not colocalize with anti-OMP (A and B). White dotted lines in (C–F) indicate the apical and basal surfaces of the epithelium. CHD7-positive cells express the pro-neuronal basal stem cell marker Mash1 and the immature olfactory sensory neuron marker NeuroD. CHD7-positive cells colocalize with nuclei of the sustentacular cell markers Reep6 and Sus1 (I and J). Arrow (I) indicates a CHD7-positive/Sus1-positive cell with a microvillar-like cell morphology.

which surround the glomeruli with anti-tyrosine hydroxylase. Tyrosine hydroxylase is expressed in these interneurons in response to signal transduction from the olfactory sensory neurons (36). We found a significant reduction in tyrosine hydroxylase label around the glomeruli in the $Chd7^{Gt/+}$ olfactory bulb (Fig. 4G and H). These data demonstrate that although $Chd7^{Gt/+}$ olfactory sensory neurons appear to project normally to the olfactory bulb, olfactory bulb interneuron activity is reduced.

Analysis of cell type-specific functions in $Chd7^{Gt}$ olfactory epithelium

The absence of response to odorants by electro-olfactogram in $Chd7^{Gt/+}$ mice demonstrates an inability of the $Chd7^{Gt/+}$ epithelium to generate or conduct an electrical current after exposure to chemical stimuli. In order to test the function of olfactory sensory neurons, we used calcium imaging in olfactory epithelium slices to analyze whether individual olfactory sensory neurons elicit a signal in response to odorants (37). We found that $Chd7^{Gt/+}$ pups had functional olfactory sensory neuron (OSN) responses to odorants similar to wild-type littermates (Fig. 5A–F). These data show that early postnatal olfactory sensory neurons are intact in $Chd7^{Gt/+}$ mice, and exclude developmental delay as a cause of mature olfactory epithelium dysfunction.

Because sustentacular cells are essential for normal olfactory function (33), we tested whether olfactory dysfunction in $Chd7^{Gt/+}$ mice was due to defects in sustentacular cells. To test this, we measured sustentacular cell function by examining glutathione *S*-transferase (GST) activity (Fig. 5G). GST expression is restricted to sustentacular cells and Bowman's glands (and not olfactory sensory neurons) in the olfactory epithelium (38,39), and is necessary for sustentacular cells to properly detoxify the olfactory environment which is under constant environmental stress (33). We found normal GST activity in $Chd7^{Gt/+}$ mice compared with wild-type littermates (Fig. 5G). Together, these data suggest a mechanism of reduced olfaction in $Chd7^{Gt/+}$ mice that is independent of GST activity in sustentacular cells, and suggest that olfactory dysfunction is not simply due to an unhealthy olfactory epithelium.

Analysis of other mouse mutants with reduced olfaction has indicated that all of the necessary components for odorant detection need to be properly localized in the cilia (40) and that proper cilia structure and function are essential for normal odorant detection (41,42). To test whether cilia structure and function are altered in $Chd7^{Gt/+}$ mice, we measured ciliary adenylyl cyclase activity and analyzed cilia by immunofluorescence with antibodies against cilia components. Adenylyl cyclase activity in the cilia is essential for canonical G-protein coupled receptor signaling in most olfactory sensory neurons (43). We detected normal basal and forskolin-stimulated adenylyl cyclase activity in adult $Chd7^{Gt/+}$ mice (Fig. 5H).

Interestingly, immunofluorescence label for cilia markers in $Chd7^{Gt/+}$ mice was consistently patchy between mice and between sections within a given mouse, with some regions appearing to have normal antibody label and other regions showing decreased label, consistent with regional differences in cilia distribution (Fig. 6A and B). We also found intact but variable immunofluorescence for several cilia components in $Chd7^{Gt/+}$ mice, including acetylated α-tubulin (Fig. 6A–D), $G_{\gamma}13$ (Fig. 6E and F), adenylyl cyclase III (Fig. 6G and H), CNGA2 and γ-tubulin (Supplementary Material, Fig. S2).

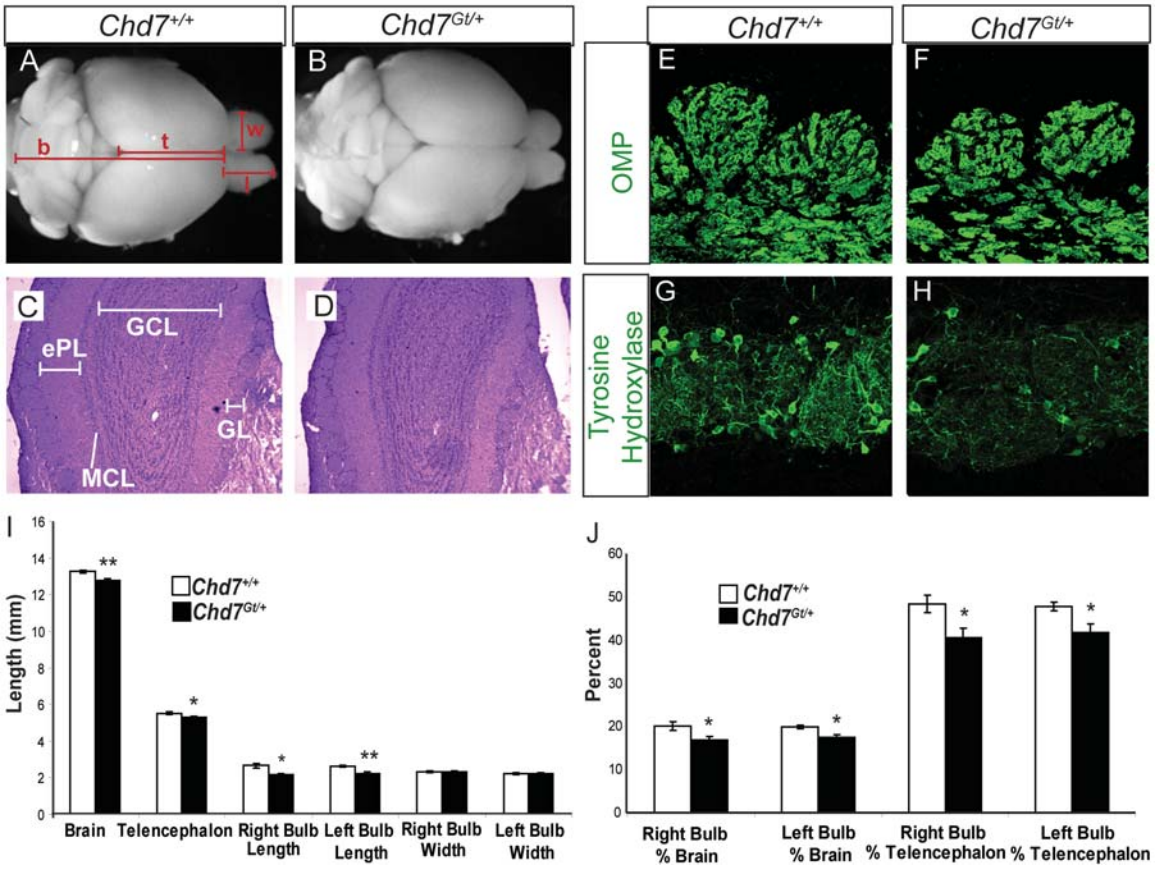

Figure 4. *Chd7* mutant mice have olfactory bulb hypoplasia. Brains were dissected and imaged from 6-week-old $Chd7^{+/+}$ ($n = 5$) and $Chd7^{Gt/+}$ mice ($n = 5$) (**A** and **B**). Measurements were taken of the brain (b), telencephalon (t), olfactory bulb length (l) and olfactory bulb width (w). $Chd7^{Gt/+}$ mice have significantly smaller brains, telencephalons and olfactory bulb lengths compared with wild-type littermates (**I**). Significant differences in olfactory bulb length taken as a percent of the brain and telencephalon indicate that *Chd7* mutant mice (closed bars) have olfactory bulb hypoplasia compared with wild-type littermates (open bars) (**J**). Cross-sections of the olfactory bulbs stained with hematoxylin and eosin (**C** and **D**) show no difference in the layer composition of $Chd7^{Gt/+}$ olfactory bulbs. Anti-OMP in the olfactory bulb stains the glomeruli in both wild-type and $Chd7^{Gt/+}$ mice (**E** and **F**). Dopaminergic interneurons surrounding the glomeruli express tyrosine hydroxylase (TH) in response to electrical activity from olfactory sensory neurons in wild-type mice, whereas TH label is decreased in $Chd7^{Gt/+}$ mice (**G** and **H**). $^{*}P < 0.05$ and $^{**}P < 0.01$ as determined by unpaired Student's *t*-test. Abbreviations: GL, glomerular layer; ePL, external plexiform layer; MCL, mitral cell layer and GCL, granule cell layer.

These data indicate that abnormalities in cilia components are not a likely contributor to reduced olfactory function in $Chd7^{Gt/+}$ mice, but that regional decreases in the amount of cilia present may potentially contribute to olfactory dysfunction.

Olfactory sensory neurons are reduced and disorganized in $Chd7^{Gt/+}$ mice

The cytoarchitecture of the postnatal olfactory epithelium is highly organized, and each cell type can be distinguished by its gene expression profile, apical–basal location and morphology. We examined the ultrastructure of the olfactory epithelium in wild-type and $Chd7^{Gt/+}$ mice using scanning electron microscopy (SEM). By SEM, we observed wild-type OSN cell bodies organized in parallel stacked columns within the epithelium (Fig. 7A). In contrast, $Chd7^{Gt/+}$ OSN cell bodies appeared to have lost this highly ordered arrangement (Fig. 7B). We also observed patchy cilia distribution on the apical surface of the $Chd7^{Gt/+}$ epithelium consistent with the immunofluorescence for cilia components (Fig. 7C and D). These data indicate that olfactory sensory neurons in $Chd7^{Gt/+}$ olfactory epithelium are disorganized but retain some dendritic projections to the apical surface.

We closely examined olfactory epithelial cell types by transmission electron microscopy (TEM). We found that wild-type and $Chd7^{Gt/+}$ olfactory sensory neurons appear to extend dendrites which end in a dendritic knob on the apical surface of the epithelium and project cilia along the nasal mucosa (Fig. 7E and F). We then directly quantified the numbers of various cell types in the olfactory epithelium by light microscopic analysis of tissues that had been processed for TEM (Fig. 7G–I). Cell types were classified based upon their location in the epithelium and their morphology. The number of cells of each type was compared with the average known percentages of each cell type of the adult olfactory epithelium: apical cells 15%, olfactory sensory neurons 75–80% and basal (globose and horizontal) cells 10% (33). The apical-most and basal-most populations of cell nuclei could not be differentiated into further subclasses. The remaining cell bodies located in the medial portion of the epithelium were counted as olfactory sensory neurons (Fig. 7G and H). We detected a significant reduction (30%) in the number of

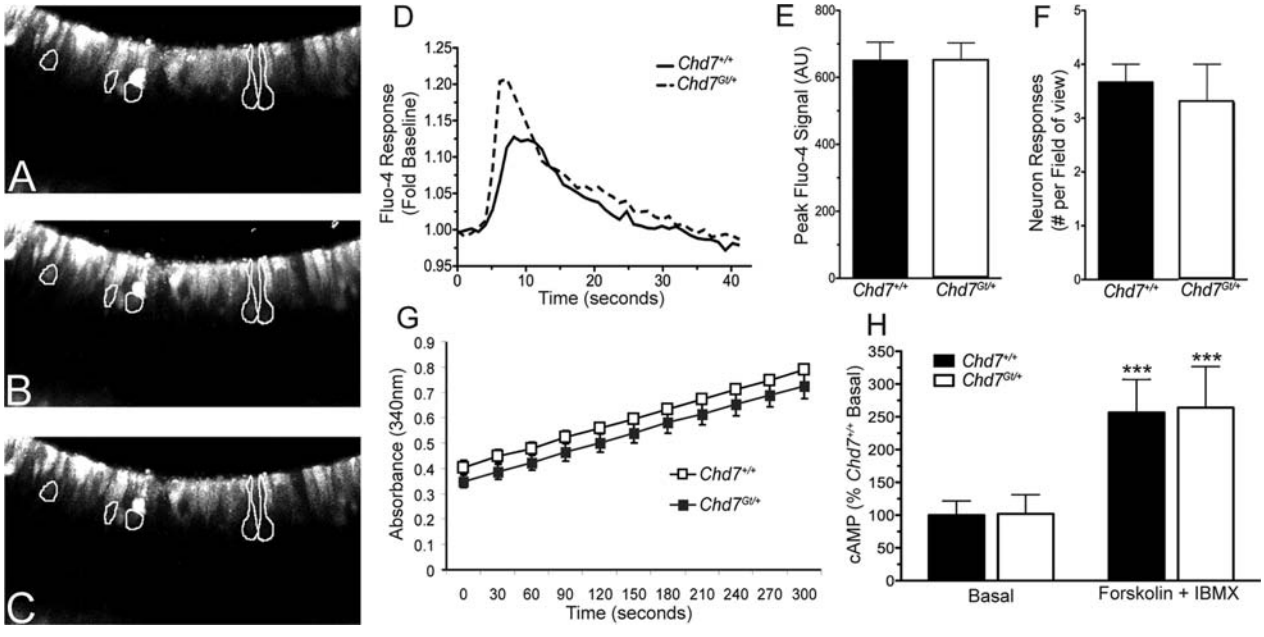

Figure 5. Olfactory sensory neurons and sustentacular cells are physiologically intact in early postnatal *Chd7*$^{Gt/+}$ mice. Odor-evoked calcium responses are similar in postnatal day 3 wild-type ($n = 4$) and *Chd7*$^{Gt/+}$ ($n = 4$) mouse olfactory epithelial slices. Representative confocal images (**A**–**C**) from a single fluo-4 AM-loaded *Chd7*$^{Gt/+}$ mouse olfactory epithelial slice (A) before, (B) during or (C) after odorant application. Representative responding neurons are outlined in (A–C). Average time course data (**D**) were generated from recordings of 22 wild-type and 23 *Chd7*$^{Gt/+}$ neurons imaged over six slices. No significant difference was observed between wild-type and *Chd7*$^{Gt/+}$ mice as determined by an unpaired Student's *t*-test. Histogram representation of the average peak odor-evoked response (**E** and **F**) of the neurons measured in (D). Glutathione *S*-transferase activity (**G**) was examined in 6-week-old wild-type (closed circles, $n = 3$) and *Chd7*$^{Gt/+}$ (closed squares, $n = 3$) mice. A representative pair of 6-week-old wild-type and *Chd7*$^{Gt/+}$ littermates showed no significant difference in sustentacular cell activity as determined by an unpaired Student's *t*-test. Adenylyl cyclase activity was examined in the presence or absence of 10 μM forskolin (**H**) in 6-week-old wild-type ($n = 8$) and *Chd7*$^{Gt/+}$ ($n = 8$) littermate mice. No significant difference was observed in either the basal or forskolin-stimulated cyclase activity as determined by an unpaired Student's *t*-test. Data are presented as the mean ± SEM from three separate experiments, where each condition was tested in duplicate. $^{***}P < 0.001$ as measured by one-way ANOVA.

olfactory sensory neurons in *Chd7*$^{Gt/+}$ mice (Fig. 7H and I), consistent with our previous observation of decreased OMP staining (Fig. 3A and B). There was also a small (10%) yet significant reduction in the number of basal cells in *Chd7*$^{Gt/+}$ mice (Fig. 7H and I). We found no statistically significant difference in the number of apical cells in *Chd7*$^{Gt/+}$ mice compared with wild-type (Fig. 7H and I). The smaller reduction in basal cells compared with the larger reduction observed in olfactory sensory neurons is likely due to the olfactory epithelium having two populations of basal cells: horizontal basal cells (HBCs) and globose basal cells (GBCs). Since HBCs are typically quiescent (33), their cell numbers may not be as influenced by reduced *Chd7* dosage as GBCs. Reduced GBCs with no change in HBCs could also skew the data toward the small difference in total basal cell number. These data indicate that the appearance of disorganized olfactory sensory neurons in *Chd7*$^{Gt/+}$ mice could be related to an overall reduction in the number of olfactory sensory neurons and GBCs.

Neural stem cell proliferation in the olfactory epithelium requires CHD7

Basal cells are the stem cell progenitors in the postnatal olfactory epithelium, and GBCs are known to be a highly dynamic pro-neuronal basal cell population (33,44–48). Since Mash1/NeuroD labeling showed that *Chd7* is expressed in pro-neuronal basal cells, we tested whether *Chd7*$^{Gt/+}$ olfactory epithelia have defects in cellular proliferation. For these studies, we used a 5-bromo-2-deoxyuridine (BrdU) incorporation assay to identify S-phase cells in the wild-type and *Chd7*$^{Gt/+}$ olfactory epithelium. Colocalization between anti-BrdU and anti-CHD7 immunofluorescence allowed us to visualize and quantify CHD7-positive and BrdU-positive proliferating basal cells (Fig. 8A–D). We found that *Chd7* is expressed in 98% of BrdU-positive proliferating basal cells in both wild-type and *Chd7*$^{Gt/+}$ mice (Fig. 8A–D). *Chd7* expression was high in crypt regions, which also appeared to be sites of high cellular proliferation in the olfactory epithelium (Fig. 8A and B). Previous reports indicate that there are regions of the olfactory epithelium where proliferation is more active (49). These crypt regions appear to have high levels of CHD7-positive proliferating basal cells. Quantification of CHD7-positive and BrdU-positive cells revealed a 50% reduction in proliferating basal cells in the olfactory epithelium in adult *Chd7*$^{Gt/+}$ mice compared with wild-type littermates (Fig. 8E). There was also a 50% reduction in the number of CHD7-positive cells in the apical region of the epithelium (Fig. 8E). Together, these data indicate a requirement for CHD7 in proliferating cells in the basal olfactory epithelium. Reduced numbers of proliferating GBCs could translate into fewer apical CHD7-positive cells and lead to fewer mature olfactory sensory neurons, as predicted by the reduced intensity of olfactory epithelium OMP staining (Fig. 3A and B).

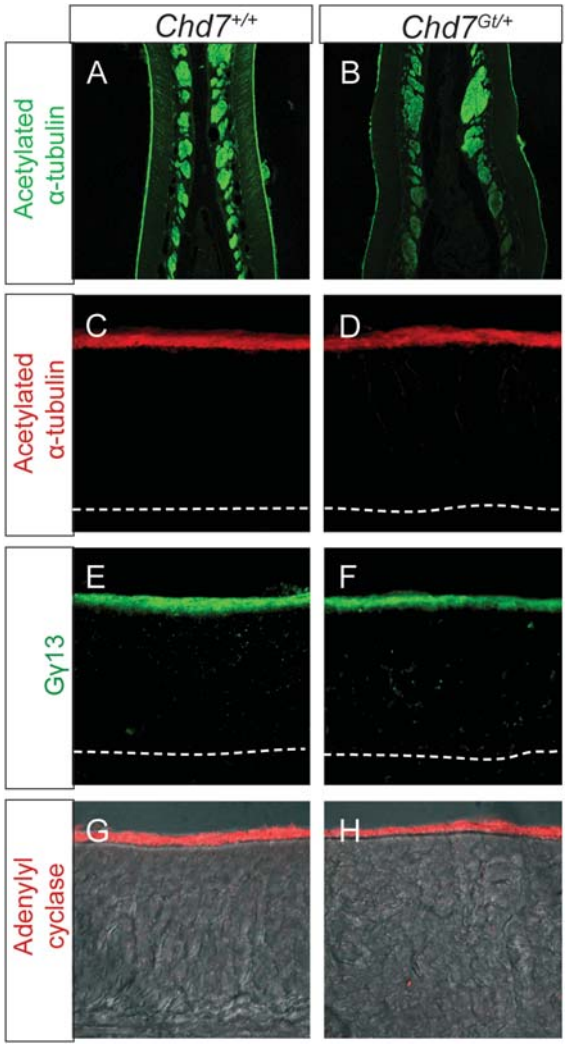

Figure 6. Components of the olfactory cilia are intact in $Chd7^{Gt/+}$ mice. Olfactory cilia proteins were labeled in wild-type and $Chd7^{Gt/+}$ mice by immunofluorescence with anti-acetylated α-tubulin (**A**–**D**), anti-$G_{\gamma}13$ (**E** and **F**) and anti-adenylyl cyclase III (**G** and **H**). Regional decreases in immunofluorescence label were consistently observed in $Chd7^{Gt/+}$ mice for all cilia markers, as represented by acetylated α-tubulin label (A and B). White dotted lines in (C–F) indicate the basal surface of the epithelium. Immunofluorescence using antibodies against cilia proteins indicated that although regional decreases in label existed, all cilia components analyzed were present in $Chd7^{Gt/+}$ olfactory cilia compared with wild-type littermates.

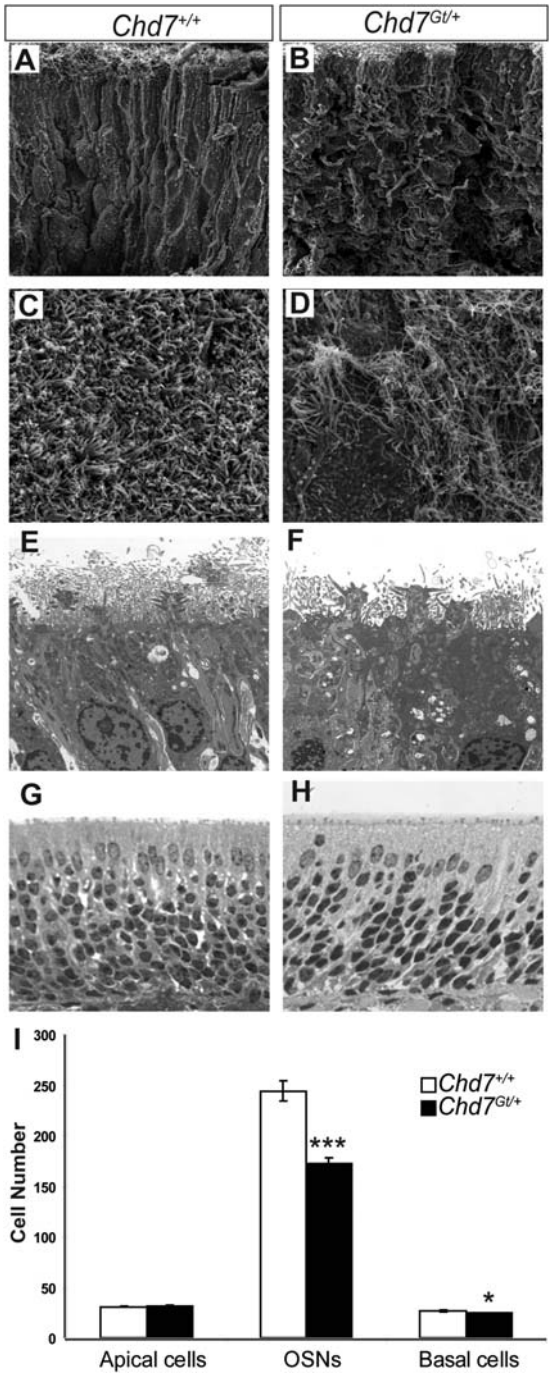

Figure 7. Olfactory sensory neurons in $Chd7^{Gt/+}$ mutant mice are disorganized and reduced in number. Scanning electron micrographs of the olfactory epithelium show loss of the orderly arrangement of olfactory sensory neurons in (**B**) $Chd7^{Gt/+}$ mice ($n = 4$) compared with (**A**) wild-type littermates (n=4). Olfactory cilia are present in wild-type and $Chd7^{Gt/+}$ mice; however, $Chd7^{Gt/+}$ mice have variable distribution of cilia on the apical surface (**C** and **D**). Transmission electron micrographs from $Chd7^{Gt/+}$ mice ($n = 3$) compared with wild-type littermates ($n = 3$) show that olfactory sensory neurons from $Chd7^{Gt/+}$ mice properly extend dendrites to the apical surface and have cilia which project along the nasal mucosa (**E** and **F**). Light microscopy of olfactory epithelial tissues processed for TEM (**G** and **H**) shows a reduction in olfactory sensory neurons. Cell counts of TEM tissue sections (**I**) show a significant reduction in $Chd7^{Gt/+}$ (closed bars) olfactory sensory neurons and basal cells compared with wild-type (open bars) littermates $^{*}P < 0.05$ and $^{***}P < 0.001$ as determined by unpaired Student's t-test. Abbreviation: OSNs, olfactory sensory neurons.

Neuronal regeneration is altered in $Chd7^{Gt/+}$ mice

Neuronal regeneration throughout adulthood is an essential characteristic for continued function of the olfactory epithelium, since the olfactory epithelium is continuously exposed to environmental stresses and must recover to maintain its primary function of odorant detection. To determine whether defects in $Chd7^{Gt/+}$ olfaction were associated with abnormalities in neuronal regeneration, we chemically ablated the olfactory epithelium and assayed neuronal regeneration in wild-type and $Chd7^{Gt/+}$ mice. 6-week-old wild-type ($n = 9$) and $Chd7^{Gt/+}$ ($n = 8$) sex-matched littermates were given a 25 μl intranasal infusion of 1% Triton X-100 in saline. At 2 weeks post-ablation, one wild-type mouse was sacrificed to determine efficiency of

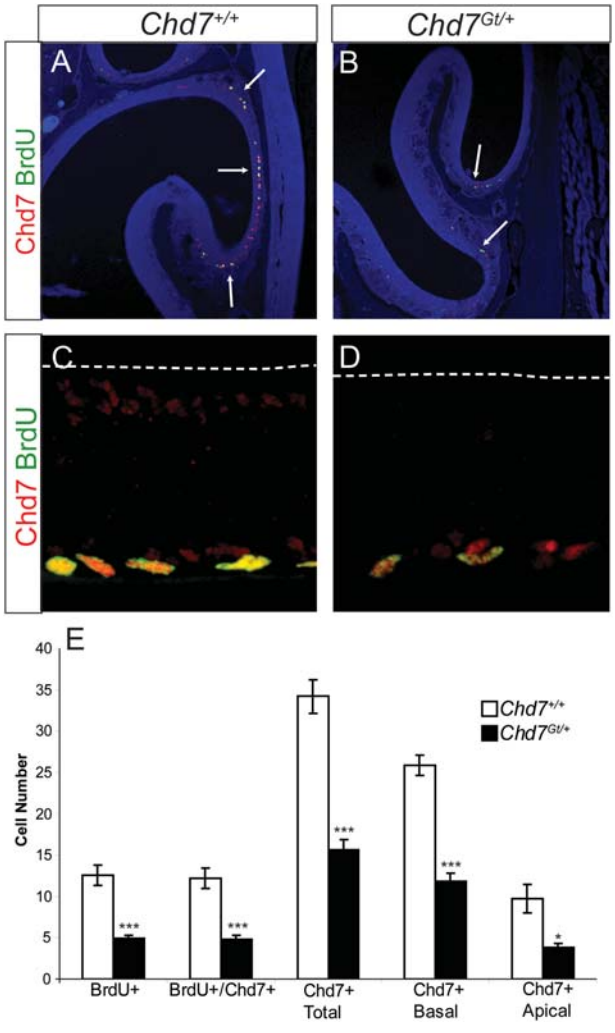

Figure 8. Olfactory epithelial basal cell proliferation is reduced in *Chd7*$^{Gt/+}$ mice. Adult wild-type and *Chd7*$^{Gt/+}$ mice were exposed to BrdU 30 min prior to tissue collection, then processed for double immunofluorescence with anti-BrdU and anti-CHD7. Many CHD7-positive basal cells are actively dividing, based on co-localization between anti-CHD7 and anti-BrdU (**A**–**D**). *Chd7* is highly expressed in crypt regions (marked by arrows) which also appear to be regions of high proliferation in the olfactory epithelium (A and B). White dotted lines in (C and D) indicate the apical surface of the epithelium. Cell counts (wild-type=open bars, *Chd7*$^{Gt/+}$=closed bars) show a 50% reduction in the number of BrdU-positive cells in the *Chd7*$^{Gt/+}$ olfactory epithelium and a 50% reduction in the number of all CHD7-positive cells (basal and apical). $^{*}P < 0.05$ and $^{***}P < 0.001$ as determined by unpaired Student's *t*-test.

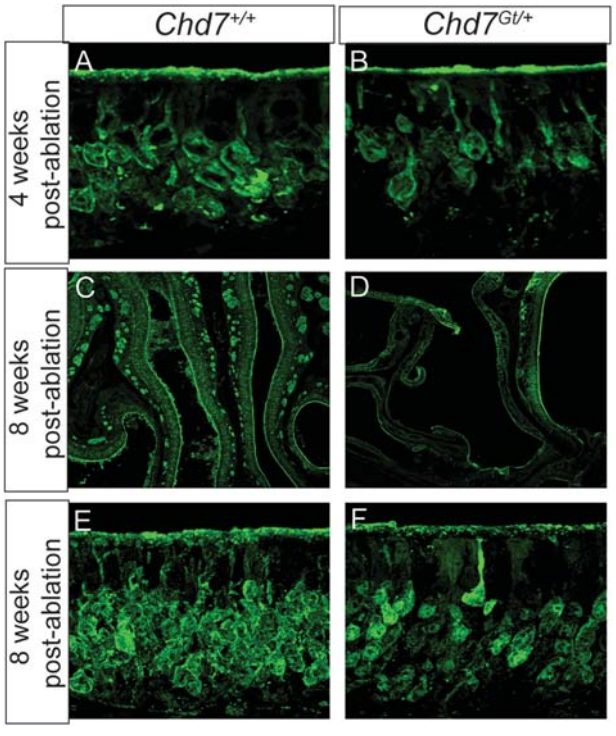

Figure 9. *Chd7*$^{Gt/+}$ mice exhibit altered regeneration of olfactory sensory neurons in the olfactory epithelium after chemical ablation. A 6-week-old wild-type ($n = 9$) and *Chd7*$^{Gt/+}$ mice ($n = 8$) were given an intranasal infusion of 1% Triton X-100 in saline then sacrificed 2, 4 or 8 weeks later. The olfactory epithelium at 4 weeks post-ablation (**A** and **B**) shows olfactory sensory neurons in both wild-type ($n = 4$) and *Chd7*$^{Gt/+}$ ($n = 4$) littermates, with some disorganization and reduced OMP label. At 8 weeks post-ablation (**C**–**F**), wild-type mice ($n = 4$) exhibit a normal appearing olfactory epithelium, whereas *Chd7*$^{Gt/+}$ mice ($n = 4$) have regionally restricted OMP staining and OSN regeneration.

the ablation technique. The olfactory epithelium was completely ablated at 2 weeks post-ablation (Supplementary Material, Fig. S3), with no observable OMP or Reep6 staining. At 4 weeks post-ablation, wild-type ($n = 4$) and *Chd7*$^{Gt/+}$ ($n = 4$) mice were sacrificed and analyzed for neuronal regeneration by immunofluorescence using anti-OMP (Fig. 9A and B). Both wild-type and *Chd7*$^{Gt/+}$ mice had some degree of OMP staining and neuronal regeneration. However, *Chd7*$^{Gt/+}$ mice had reduced OMP-positive cells which also appeared to be disorganized compared with wild-type littermates. At 8 weeks post-ablation, wild-type ($n = 4$) mice had almost complete recovery of olfactory sensory neurons in the olfactory epithelium (Fig. 9C and E), whereas *Chd7*$^{Gt/+}$ ($n = 4$) mice had regional differences in neuronal regeneration with some regions of the epithelium appearing normal, whereas others exhibited little to no neuronal regeneration (Fig. 9D and F). These data indicate that adult *Chd7*$^{Gt/+}$ mice have delayed or impaired ability to regenerate the olfactory epithelium compared with wild-type mice. Delays or reductions in the ongoing formation of new olfactory sensory neurons under normal conditions could also contribute to the olfactory defects observed in *Chd7*$^{Gt/+}$ mice.

DISCUSSION

Here, we have shown that both humans and mice with *CHD7* deficiency have impaired olfaction. We observed *Chd7* expression during development in restricted cell types of the olfactory epithelium and olfactory bulb, and *Chd7* expression in the adult mouse olfactory epithelium in proliferating basal cells and in pro-neuronal basal cells. We also found that *Chd7* deficient mice have a significant reduction in basal cell proliferation, which translates into a reduction in both basal cells and olfactory sensory neurons. Figure 10 depicts a diagram of the olfactory epithelium in both wild-type and *Chd7* mutant mice. The reduction in olfactory sensory neurons caused by *Chd7*

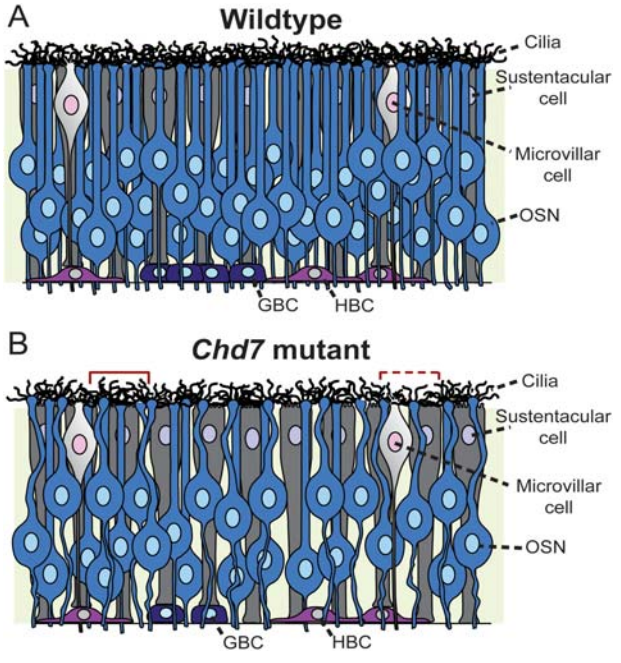

Figure 10. Diagram of the *Chd7* mutant mouse olfactory epithelium. Wild-type (**A**) and *Chd7* mutant (**B**) mouse olfactory epithelium is depicted with all of the main cell types including olfactory sensory neurons (blue), sustentacular cells (dark gray), globose basal cells (GBCs; purple), horizontal basal cells (HBCs; pink) and microvillar cells (white). *Chd7* mutant mice have ~30% fewer olfactory sensory neurons and 50% fewer GBCs compared with wild-type. Red bars indicate regions of normal cilia density (solid) and sparse cilia density (dashed). *Chd7* mutants have fewer olfactory sensory neurons, which causes gaps between the olfactory sensory neurons and a loss of support leading to a disorganized appearance. Abbreviation: OSNs, olfactory sensory neurons.

deficiency leads to regional variability in cilia density and disorganization of the *Chd7* mutant olfactory epithelium, which may influence tight junctions required for signal transduction. Additionally, *Chd7* deficient mice have a reduced capacity for regeneration of olfactory sensory neurons following chemical ablation of the olfactory epithelium. These data together suggest a critical role for *CHD7* in olfactory tissues not only during development but also into adulthood.

Our data provide the first evidence that CHD7 functions in cellular proliferation and neuronal differentiation in the olfactory epithelium. The mechanism by which CHD7 regulates cell cycle progression and stem cell differentiation is not yet understood. DNA chromatin structure has a vital role in gene regulation, cellular proliferation and maintenance of the differentiated state. However, little is known about the cell and tissue specific functions of chromodomain proteins. Protein–protein interactions involving cell cycle progression and gene expression have been reported for some CHD family members (50–56). Proteins such as histone deacetylases and nuclear receptor corepressor 1 are involved in protein interactions with CHD proteins (50–56) and are also known to be critical for neuronal differentiation (57,58). In a recent study using ChIP–chip analysis, CHD7 was shown to bind to methylated histone H3 K4 enhancer regions of numerous genes in the mammalian genome (59). These data suggest a role for CHD7 in regulating transcription, potentially affecting multiple developmental processes during cell fate specification.

CHD7 and other chromodomain proteins are also thought to regulate access to chromatin by binding and unwinding it (25–29). CHD7 could work in conjunction with other transcription factors involved in cell cycle progression and neuronal differentiation. Otx2, a paired-like homeodomain transcription factor, is critical for normal cellular proliferation and neuronal differentiation (60). *Otx2* mutant mice lack the pro-neuronal transcription factor *Mash1* (60). Mash1 induces the expression of later bHLH transcription factors like *Ngn1* and *NeuroD*, driving cell cycle exit and neuronal differentiation (33). We found that CHD7 colocalizes with BrdU-positive proliferating cells and with Mash1 and NeuroD in basal cells. Since Otx2 is involved in cellular proliferation and induces the expression of Mash1 and NeuroD, CHD7 may be necessary for access to Otx2 target genes in the olfactory epithelium. Our data indicate that *Chd7* deficiency may impact the expression and/or function of transcription factors dependent upon CHD7 for access to target genes through chromatin modifications.

Neural progenitor cells in the adult olfactory epithelium possess an extensive capacity for ongoing cellular proliferation and differentiation. These neural progenitors must be tightly regulated developmentally, temporally and spatially to maintain the integrity of the epithelium over time. *Chd7* is expressed in both the embryonic and adult olfactory epithelium, and targets of CHD7 are likely to include factors involved in the regulation of neurogenesis, neuronal regeneration and cell cycle progression. CHD7 could be involved in the expression of morphogens such as the bone morphogenetic proteins (BMPs) or fibroblast growth factors (FGFs). Previous studies have shown that BMP4 has dosage dependent opposing effects on neurogenesis in the olfactory epithelium (61,62). BMP2, BMP4 and BMP7 at high concentrations have anti-neurogenic effects on progenitors (61,62). However, low concentrations of BMP4 increase neurogenesis in the olfactory epithelium, whereas BMP2 and BMP7 retain their anti-neurogenic effects at low concentrations (61,62). Although low concentrations of BMP4 increase neurogenesis in the olfactory epithelium, BMP4 does not cause an increase in cellular proliferation (61), in contrast to the decreased cellular proliferation we observed with *Chd7* deficiency. FGF2 induces neurogenesis and increases cellular proliferation of progenitors in the olfactory epithelium (61). Together these data suggest that BMP and FGF signaling may be sensitive to changes in *CHD7* dosage in the olfactory epithelium.

Interestingly, *Chd7* deficiency does not appear to affect the structure, function or localization of olfactory cilia components. However, we observed regional cilia reductions in $Chd7^{Gt/+}$ mice that could contribute to defects in odorant detection. These data indicate that unlike other mouse models with defects in olfaction, olfactory dysfunction in $Chd7^{Gt/+}$ mice is not caused by defects in cilia structure, function (41,42) or protein transport (40). Instead, reduced numbers of olfactory sensory neurons and cilia could contribute to impaired olfaction in mature $Chd7^{Gt/+}$ mice, perhaps through altered electrical signal transmission. The apparently normal calcium responses in neurons of the neonatal *Chd7* mutant mouse olfactory epithelium suggest that the developing mutant epithelium is relatively normal. Therefore, later defects in electro-olfactogram, olfactory bulb tyrosine hydroxylase label, reduced olfactory bulb size and reduced olfactory performance in CHARGE

patients could be a result of ongoing abnormalities in neural stem cell proliferation and reduced/disorganized olfactory sensory neurons. Future studies of developing *Chd7* mutant olfactory tissues and olfactory behaviors in *Chd7* mutant mice should help to clarify these pleiotropic effects.

Olfactory dysfunction in CHARGE has typically been associated with defects in the olfactory bulb which ranged from hypoplasia to complete absence of one or both lobes of the olfactory bulb (15–20). *Chd7* mutant mice have olfactory bulb hypoplasia, consistent with the observed human phenotype. However, the olfactory bulb defects observed in CHARGE individuals often consist of more severe hypoplasia or complete absence of one or both olfactory bulb lobes. Since we detected olfactory hypoplasia in young adult mice (6 weeks), it is also possible that the olfactory bulb hypoplasia could become progressively more severe as the animals age. Defects in the olfactory epithelium have not previously been analyzed in humans or mice with *CHD7* mutations (15–20). We found that $Chd7^{Gt/+}$ mice have severely impaired olfaction by electro-olfactogram, which measures odorant detection directly from the surface of the epithelium independent of the olfactory bulb. Our data indicate that olfactory dysfunction in CHARGE individuals may be attributed to primary defects in the olfactory epithelium, and raise the possibility that reduced sensory input from olfactory sensory neurons could contribute to later and more severe olfactory bulb defects.

Prior studies of olfaction in CHARGE have also been limited because the mutation status of the individuals was not reported (15–18,20) in all but one study of a female with CHARGE and Kallmann (19), and in a recent report of three individuals ascertained on the basis of a Kallmann syndrome phenotype (63). The eight patients in our study have *CHD7* mutations that span the gene and one functional domain (SNF domain) of the CHD7 protein (Table 1). Our study is the first report of measured reduction in olfaction in CHARGE patients with known *CHD7* mutations. We chose the B-SIT to analyze olfactory dysfunction in CHARGE individuals, because it is a rapid test that is readily available and inexpensive, especially compared with physiological measures of olfactory function in humans (64). The B-SIT is easy to perform, even for children. However, the B-SIT is not reliable for distinguishing degrees of hyposmia and anosmia (64). Also, our results could be potentially influenced by cognitive impairment, as is true for the University of Pennsylvania Smell Identification Test, from which the B-SIT is based. Our B-SIT data were obtained from individuals who took the test at home, which could also have influenced test results. Despite these limitations, the B-SIT showed reduced olfaction in a majority of *CHD7* mutation-positive CHARGE individuals. A better understanding of the mechanisms involved in the pathogenesis of CHARGE will help facilitate both diagnosis and therapies for CHARGE syndrome. Our data suggest that the B-SIT could be used in a clinical setting as an additional diagnostic tool for evaluating children and adults with suspected CHARGE phenotypes.

We have identified a novel role for CHD7 in neural stem cells of the olfactory epithelium, which could provide insight into a similar role for *Chd7* in regulating cell cycle and cell fate specification in other sensory and non-sensory tissues. Our data also demonstrate a novel mechanism for olfactory dysfunction in mammals caused by reduced olfactory sensory neurons. How does a reduction in olfactory sensory neurons lead to impaired olfaction? We hypothesize that fewer olfactory sensory neurons are insufficient to generate an electrical potential, leading to reduced neuronal electrical transmission to the olfactory bulb. Reduced tyrosine hydroxylase in the $Chd7^{Gt/+}$ olfactory bulb is consistent with this notion. A reduction in olfactory sensory neurons in $Chd7^{Gt/+}$ mice may also alter the integrity of the olfactory epithelium such that critical cell–cell contacts are disrupted, impairing the ability of the olfactory sensory neurons to process and maintain electrical signals. It will be important to identify whether there are critical genes dysregulated by loss of *Chd7* function. We expect some genes regulated by CHD7 to influence proliferation, whereas others may control aspects of cellular differentiation. Generation and characterization of conditional *Chd7* null mutants could also enable further analysis of the roles of CHD7 during olfactory development. Since *Chd7* null mice are embryonic lethal by E11 (21,22), tissue specific and inducible knockouts would enable research on homozygous phenotypes that are currently not amenable for study in heterozygous mouse models. Our work also opens new questions for future research on the function of CHD7 in stem cells in the olfactory system and elsewhere.

MATERIALS AND METHODS

Human olfactory testing

We used the B-SIT (Brief Smell Identification Test™, Sensonics, Inc., Haddon Heights, NJ, USA) as a measure of olfactory function in individuals with CHARGE syndrome. The B-SIT is a 12 item self-administered test booklet which contains odorants embedded on scent strips that are released by scratching with a pencil (40,64–67). Answers are given as multiple choices among four alternative responses. Individuals with CHARGE who were 10 years or older, and their parents or unaffected siblings, were recruited for participation by mail inquiries, and then subsequently sent test booklets for scoring. Individuals were provided with detailed instructions for completing the test. All aspects of the study were approved by the IRB medicine review committees of the University of Michigan and Baylor College of Medicine.

Mice

$Chd7^{Gt/+}$ mice were generated by backcrossing with 129S1/Sv1mJ (Jackson Laboratory) mice to generation N5–N7 and genotyped using methods as previously described (22). We found no detectable CHD7 immunofluorescence in $Chd7^{Gt/Gt}$ E10.5 embryos using a polyclonal anti-CHD7 antibody, confirming that $Chd7^{Gt}$ is a null allele (unpublished data). All procedures were approved by University Committee on Use and Care for Animals at the University of Michigan and Michigan State University.

Immunofluorescence

A 6-week-old $Chd7^{+/+}$ and $Chd7^{Gt/+}$ sex-matched littermate mice were anaesthetized with 250 mg/kg body weight tribromoethanol and perfusion fixed with 4% paraformaldehyde.

Mice were then decapitated and heads placed in 4% paraformaldehyde overnight at 4°C. Heads were incubated in RDO Rapid Decalcifier (Apex Engineering, Aurora, IL, USA) for 4–6 h followed by 30% sucrose protection overnight at 4°C. Tissue was flash frozen in O.C.T. embedding medium (Tissue Tek, Torrance, CA, USA) for sectioning. Following cryosectioning, 14 μm sections were processed for hematoxylin/eosin staining or immunofluorescence with antibodies against adenylyl cyclase III (1:500; Santa Cruz, Santa Cruz, CA, USA), CNGA2 (1:200; Alomone Labs, Jerusalem, Israel), acetylated α-tubulin (1:1000; Sigma, St Louis, MO, USA), $G_{\gamma}13$ (1:200; gift of Robert Margolskee, Mt. Sinai School of Medicine, New York, NY, USA), γ-tubulin (1:500; Sigma), OMP (1:200; Wako Chemicals USA, Inc., Richmond, VA, USA), CHD7 (1:1000; Abcam, Cambridge, MA, USA), β-galactosidase (1:1000; gift of Thomas Glaser), BrdU (1:100; Immunologicals Direct, Raleigh, NC, USA), NeuroD (1:1000; gift of Jacques Drouin), Mash1 (1:150; Abcam), Tyrosine hydroxylase (1:150; Pel-Freez, Rogers, AR, USA), Sus1 (1:20; gift of Frank Margolis) or Reep6 (1:500). Rabbit anti-sera against mouse REEP6 peptides (1–16; MDGLRQRFERFLEQKN and 188–201; STSEPPAALELDPK) were generated by Zymed Laboratories Inc. (South San Francisco, CA, USA). Specificity to REEP6 was confirmed in cell-based transfection assays. Secondary antibodies used at 1:200 were conjugated with Alexa 488, Alexa 555 or biotin with streptavidin-HRP (Vector Laboratories) and biotinylated secondary antibodies conjugated with streptavidin-Alexa488 or streptavidin-Alexa555 (Molecular Probes, Eugene, OR, USA and Invitrogen, Carlsbad, CA, USA). NIH ImageJ software (Bethesda, MD, USA) was used to analyze fluorescence intensity over at least 30 images. Fluorescence intensity was measured in restricted areas of the epithelium encompassing the olfactory sensory neurons but excluding cilia label, and background was subtracted to obtain the final measurements. Images were captured on a confocal microscope (Olympus IX-81 inverted scope) using the Olympus FluoView 500 software and processed in Photoshop CS2 version 9.0.

β-Galactosidase assay

Timed pregnancies were established between *Chd7*$^{Gt/+}$ and wild-type mice, with the morning of plug identification designated E0.5. Embryos were collected at E12.5 after cervical dislocation and hysterectomy. Embryos were briefly washed in PBS and amniotic sacs were collected for DNA isolation and PCR genotyping. Embryos were processed for X-gal staining as previously described (68). X-gal stained sections were post-fixed in 4% paraformaldehyde and counterstained in eosin. Sections were visualized with a Leica DMRA microscope and digital images processed with Adobe Photoshop CS2 V9.0 software.

Proliferation assays

Mice were injected intraperitoneally with 0.1 g/g body weight BrdU 30 min prior to sacrifice. Tissues were then processed for anti-BrdU and anti-CHD7 immunofluorescence as above. Secondary antibodies were conjugated with Alexa 488, Alexa 555 or biotin, as above. For quantitation of S-phase cells, confocal images from three regions of the olfactory epithelium were analyzed in eight different mice ($n = 4$ wild-type, $n = 4$ *Chd7*$^{Gt/+}$ sex-matched littermates). From each tissue section, 4–6 images were analyzed using Olympus FluoView 500 software for number of CHD7-positive, BrdU-positive and CHD7/BrdU-positive cells, and the data tested for significance by *t*-test using two-tailed unequal variance.

Scanning and TEM

A 6-week-old *Chd7*$^{+/+}$ and *Chd7*$^{Gt/+}$ sex-matched littermate mice were anaesthetized with 250 mg/kg body weight tribromoethanol and perfusion fixed with 2% glutaraldehyde. Mice were decapitated, the head bisected along the midline and further dissected to expose the olfactory epithelium. The olfactory epithelium was dissected from the head and fixed in 2% glutaraldehyde overnight. The tissue was then prepared for SEM using the OTOTO fixation method (69). SEM was performed at the University of Michigan Microscope and Image Analysis Laboratory using the AMRAY 1910 Field Emission Scanning Electron Microscope.

For TEM, perfusion fixed and dissected olfactory tissues were processed for TEM as previously described (70–72). TEM was done at the University of Michigan Microscope and Imaging Analysis Laboratory using the Philips CM-100 transmission electron microscope. For quantifying numbers of cells in the olfactory epithelium, tissues processed for TEM were sectioned (1 μm). Olfactory tissue sections from each pair of littermate mice ($n = 3$ wild-type, $n = 3$ *Chd7*$^{Gt/+}$ sex-matched littermates) were collected randomly from three different regions of the epithelium. Within each section, cells in 10 images were counted, taking into consideration their location in the epithelium and their cellular morphology. Sections were visualized with a Leica DMRA microscope and digital images processed with Adobe Photoshop CS2 V9.0 software. Cell numbers were analyzed for significance by *t*-test using two-tailed unequal variance.

Electro-olfactograms

A 6-week-old *Chd7*$^{+/+}$ and *Chd7*$^{Gt/+}$ sex-matched littermate mice were sacrificed by CO_2 inhalation then decapitated, the head bisected along the midline, and tissues dissected to expose the turbinates of the olfactory epithelium. Electrodes ranging from 4 to 8 MΩ in resistance filled with Ringers containing 0.1% agarose were placed on either turbinates II or IIb for recording. Vapor-phase odor stimuli were generated from 10 ml of solution in a sealed 50 ml bottle. The odorants were delivered as a 20 ml pulse injected into a continuous stream of humidified air flowing over the tissue sample. The data were then analyzed with Clampfit (Molecular Devices Corporation, Sunnyvale, CA, USA) and peak heights determined from pre-pulse baseline. Data were normalized to a pulse of pure amyl acetate given later in the same trace. *Chd7* mutant data were normalized to the average response of the *Chd7* wild-type mouse for a specific dose of the odorant. For each mouse tested ($n = 8$ wild-type, $n = 7$ *Chd7*$^{Gt/+}$ sex-matched littermates), four different concentrations of amyl acetate were delivered as well as five

additional odorants (octanal, heptaldehyde, hexanal, eugenol and carvone) each tested at a concentration of 10^{-3} M of the respective odorant.

Adenylyl cyclase/cAMP accumulation assay

A 6-week-old *Chd7*$^{+/+}$ and *Chd7*$^{Gt/+}$ sex-matched littermate mice were sacrificed by CO_2 inhalation then decapitated. Cilia membranes were isolated essentially as described previously (73). Briefly, olfactory epithelia from either wild-type or *Chd7*$^{Gt/+}$ mice were dissected into small pieces. Cilia were removed from the epithelium by agitation in Ringers solution supplemented with 10 mM $CaCl_2$ and Complete Protease Inhibitor tablets (Roche, Indianapolis, IN, USA). Tissue was rocked for 15 min at 4°C followed by centrifugation at 7700*g* for 5 min. The supernatant was collected in a separate tube and the agitation/centrifugation steps were repeated two more times. The pooled supernatants were centrifuged for 30 min at 27 000*g* to pellet the ciliary membranes. The supernatants were discarded and the pellet was resuspended in GTPγS buffer (100 mM NaCl, 5 mM $MgCl_2$, 20 mM Tris–Cl, 0.8 mM EDTA, pH 7.4) supplemented with Complete Protease Inhibitors.

To start the adenylyl cyclase assay, 15–20 μg of the isolated cilia prep was added to the assay mix containing 1× GTPγS buffer, 1× ATP regenerating mix, 10 μM GTP and 1 mM IBMX in the presence or absence of 10 μM forskolin. After 10 min at 37°C, the reaction was stopped by replacing the medium with ice-cold 3% perchloric acid. After at least 30 min at 4°C, 0.4 ml was removed from each sample, neutralized with 0.08 ml of 2.5 M $KHCO_3$, vortexed and centrifuged at 15 000*g* for 1 min. A 20 μl aliquot was taken from the supernatant of each sample, and accumulated cAMP was quantified using a [^{3}H]cAMP assay kit according to manufacturer's instructions (GE Healthcare, Chalfont St Giles, Buckinghamshire, UK). The total picomole cAMP produced per milligram protein was calculated for each condition. All data are presented as a percent of basal, unstimulated cyclase activity for the wild-type mouse. Statistical significance was determined using one-way ANOVA with GraphPad Prism 5 software.

Calcium imaging

Slices were essentially prepared as previously described (37). Neonatal mice (postnatal day 1–2) were sacrificed by decapitation and the lower jaw was removed. Tissue was mounted onto a vibratome-cutting block, supported by carrots and 400 μm thick slices were cut. Ice-cold slices were transferred to oxygenated Ringer solution until ready to load with dye. Ringer solution contained 140 mM NaCl, 5 mM KCl, 1 mM $MgCl_2$, 2 mM $CaCl_2$, 10 mM HEPES, 10 mM glucose and 0.5 mM probenicid (to prevent dye loss). To identify the presence of the *lacZ* gene in the heterozygous mice, one slice from each mouse was incubated in fluorescein digalactoside (Invitrogen) according to manufacturers instruction to test for β-galactosidase activity. Genotyping was confirmed by PCR analysis of genomic DNA isolated from the mouse tail snips. Prior to calcium imaging, all slices were loaded with 18 μM fluo-4 AM (Invitrogen) for 60–90 min at 25°C.

Fluo-4 loaded olfactory epithelial slices in a laminar flow chamber (Warner Instruments, Hamden, CT) were measured for odorant-evoked calcium using laser scanning confocal imaging as described previously (37). Ringer solution was continuously perfused over the slice at a flow rate of 1.5–2.0 ml/min throughout the length of the experiment. Images were taken at least 100 μm below the top of the slice to avoid damaged neurons. An odorant mixture consisting of 200 μM each of amyl acetate, carvone, eugenol, cineole, octanal, heptanal and hexanal was made fresh in Ringer solution was applied using bath exchange and a 200 μl volume loop injector. Images were acquired on an Olympus FluoView 1000 confocal laser scanning system and data analysis were performed using Olympus software and NIH ImageJ. Images were acquired approximately every 1 s for 2–3 min. For all traces, odorant was added after 15 s of recording to allow for baseline stabilization, and all data were normalized to the average of the first 15 s of recording during which odorant was absent.

GST assay

A 6-week-old *Chd7*$^{+/+}$ and *Chd7*$^{Gt/+}$ sex-matched littermate mice were sacrificed by CO_2 inhalation then decapitated. Heads were bisected along the midline to expose the olfactory epithelium. The olfactory epithelium was dissected from the head and processed for GST enzymatic activity using the GST Assay Kit as per manufacturer's instructions (Sigma).

Olfactory epithelium chemical ablation studies

A 6-week-old *Chd7*$^{+/+}$ and *Chd7*$^{Gt/+}$ sex-matched littermate mice were anesthetized with 100 mg/kg ketamine/10 mg/kg xylazine intraperitoneal injection and given a single intranasal irrigation with 20 μl of 1% Triton X-100 in 0.15 M NaCl, based on methods previously described (36). Mice were sacrificed at 2, 4 and 8 weeks post-ablation and processed for immunofluorescence using anti-CHD7, anti-OMP and anti-BrdU as described above.

SUPPLEMENTARY MATERIAL

Supplementary Material is available at *HMG* online.

ACKNOWLEDGEMENTS

The authors thank all of the families that participated in our olfactory testing and John Belmont for helpful discussions and assistance with patient recruitment. We also thank Jacques Drouin at the Institut de Recherches Cliniques de Montréal for the use of the NeuroD antibody, Thomas Glaser at the University of Michigan for providing the β-galactosidase antibody and Frank Margolis at the University of Maryland for the SUS-1 antibody. We are grateful to Karen Steel, Anne Hansen, Miriam Meisler, Jeff Innis and Sally Camper for insightful discussions.

Conflict of Interest statement. None declared.

FUNDING

This work was supported by the National Institutes of Health (RO1 NS054784 to D.M.M., RO1 DC009410 to D.M.M. and Y.R. and RO1 DC009606 to J.R.M.), the Amendt Heller Award from the University of Michigan Department of Pediatrics to D.M.M. and a Hearing Balance and Chemical Senses Training Grant from the National Institutes of Health (T32 DC00011 to W.S.L.).

REFERENCES

1. Harris, J., Robert, E. and Kallen, B. (1997) Epidemiology of choanal atresia with special reference to the CHARGE association. *Pediatrics*, **99**, 363–367.
2. Issekutz, K.A., Graham, J.M. Jr, Prasad, C., Smith, I.M. and Blake, K.D. (2005) An epidemiological analysis of CHARGE syndrome: preliminary results from a Canadian study. *Am. J. Med. Genet. A*, **133**, 309–317.
3. Kallen, K., Robert, E., Mastroiacovo, P., Castilla, E.E. and Kallen, B. (1999) CHARGE Association in newborns: a registry-based study. *Teratology*, **60**, 334–343.
4. Hall, B.D. (1979) Choanal atresia and associated multiple anomalies. *J. Pediatr.*, **95**, 395–398.
5. Aramaki, M., Udaka, T., Kosaki, R., Makita, Y., Okamoto, N., Yoshihashi, H., Oki, H., Nanao, K., Moriyama, N., Oku, S. *et al.* (2006) Phenotypic spectrum of CHARGE syndrome with CHD7 mutations. *J. Pediatr.*, **148**, 410–414.
6. Jongmans, M.C., Admiraal, R.J., van der Donk, K.P., Vissers, L.E., Baas, A.F., Kapusta, L., van Hagen, J.M., Donnai, D., de Ravel, T.J., Veltman, J.A. *et al.* (2006) CHARGE syndrome: the phenotypic spectrum of mutations in the *CHD7* gene. *J. Med. Genet.*, **43**, 306–314.
7. Lalani, S.R., Safiullah, A.M., Fernbach, S.D., Harutyunyan, K.G., Thaller, C., Peterson, L.E., McPherson, J.D., Gibbs, R.A., White, L.D., Hefner, M. *et al.* (2006) Spectrum of CHD7 mutations in 110 individuals with CHARGE syndrome and genotype–phenotype correlation. *Am. J. Hum. Genet.*, **78**, 303–314.
8. Sanlaville, D., Etchevers, H.C., Gonzales, M., Martinovic, J., Clement-Ziza, M., Delezoide, A.L., Aubry, M.C., Pelet, A., Chemouny, S., Cruaud, C. *et al.* (2006) Phenotypic spectrum of CHARGE syndrome in fetuses with CHD7 truncating mutations correlates with expression during human development. *J. Med. Genet.*, **43**, 211–217.
9. Sanlaville, D. and Verloes, A. (2007) CHARGE syndrome: an update. *Eur. J. Hum. Genet.*, **15**, 389–399.
10. Vissers, L.E., van Ravenswaaij, C.M., Admiraal, R., Hurst, J.A., de Vries, B.B., Janssen, I.M., van der Vliet, W.A., Huys, E.H., de Jong, P.J., Hamel, B.C. *et al.* (2004) Mutations in a new member of the chromodomain gene family cause CHARGE syndrome. *Nat. Genet.*, **36**, 955–957.
11. Vuorela, P., Ala-Mello, S., Saloranta, C., Penttinen, M., Poyhonen, M., Huoponen, K., Borozdin, W., Bausch, B., Botzenhart, E.M., Wilhelm, C. *et al.* (2007) Molecular analysis of the *CHD7* gene in CHARGE syndrome: identification of 22 novel mutations and evidence for a low contribution of large CHD7 deletions. *Genet. Med.*, **9**, 690–694.
12. Delahaye, A., Sznajer, Y., Lyonnet, S., Elmaleh-Berges, M., Delpierre, I., Audollent, S., Wiener-Vacher, S., Mansbach, A.L., Amiel, J., Baumann, C. *et al.* (2007) Familial CHARGE syndrome because of CHD7 mutation: clinical intra- and interfamilial variability. *Clin. Genet.*, **72**, 112–121.
13. Jongmans, M.C., Hoefsloot, L.H., van der Donk, K.P., Admiraal, R.J., Magee, A., van de Laar, I., Hendriks, Y., Verheij, J.B., Walpole, I., Brunner, H.G. *et al.* (2008) Familial CHARGE syndrome and the *CHD7* gene: a recurrent missense mutation, intrafamilial recurrence and variability. *Am. J. Med. Genet. A*, **146**, 43–50.
14. Vuorela, P.E., Penttinen, M.T., Hietala, M.H., Laine, J.O., Huoponen, K.A. and Kääriäinen, H.A. (2008) A familial CHARGE syndrome with a CHD7 nonsense mutation and new clinical features. *Clin. Dysmorphol.*, **17**, 249–253.
15. Asakura, Y., Toyota, Y., Muroya, K., Kurosawa, K., Fujita, K., Aida, N., Kawame, H., Kosaki, K. and Adachi, M. (2008) Endocrine and radiological studies in patients with molecularly confirmed CHARGE syndrome. *J. Clin. Endocrinol. Metab.*, **93**, 920–924.
16. Azoulay, R., Fallet-Bianco, C., Garel, C., Grabar, S., Kalifa, G. and Adamsbaum, C. (2006) MRI of the olfactory bulbs and sulci in human fetuses. *Pediatr. Radiol.*, **36**, 97–107.
17. Blustajn, J., Kirsch, C.F., Panigrahy, A. and Netchine, I. (2008) Olfactory anomalies in CHARGE syndrome: imaging findings of a potential major diagnostic criterion. *AJNR Am. J. Neuroradiol.*, **29**, 1266–1269.
18. Chalouhi, C., Faulcon, P., Le Bihan, C., Hertz-Pannier, L., Bonfils, P. and Abadie, V. (2005) Olfactory evaluation in children: application to the CHARGE syndrome. *Pediatrics*, **116**, e81–e88.
19. Ogata, T., Fujiwara, I., Ogawa, E., Sato, N., Udaka, T. and Kosaki, K. (2006) Kallmann syndrome phenotype in a female patient with CHARGE syndrome and CHD7 mutation. *Endocr. J.*, **53**, 741–743.
20. Pinto, G., Abadie, V., Mesnage, R., Blustajn, J., Cabrol, S., Amiel, J., Hertz-Pannier, L., Bertrand, A.M., Lyonnet, S., Rappaport, R. *et al.* (2005) CHARGE syndrome includes hypogonadotropic hypogonadism and abnormal olfactory bulb development. *J. Clin. Endocrinol. Metab.*, **90**, 5621–5626.
21. Bosman, E.A., Penn, A.C., Ambrose, J.C., Kettleborough, R., Stemple, D.L. and Steel, K.P. (2005) Multiple mutations in mouse Chd7 provide models for CHARGE syndrome. *Hum. Mol. Genet.*, **14**, 3463–3476.
22. Hurd, E.A., Capers, P.L., Blauwkamp, M.N., Adams, M.E., Raphael, Y., Poucher, H.K. and Martin, D.M. (2007) Loss of Chd7 function in gene-trapped reporter mice is embryonic lethal and associated with severe defects in multiple developing tissues. *Mamm. Genome*, **18**, 94–104.
23. Shur, I. and Benayahu, D. (2005) Characterization and functional analysis of CReMM, a novel chromodomain helicase DNA-binding protein. *J. Mol. Biol.*, **352**, 646–655.
24. Woodage, T., Basrai, M.A., Baxevanis, A.D., Hieter, P. and Collins, F.S. (1997) Characterization of the CHD family of proteins. *Proc. Natl Acad. Sci. USA*, **94**, 11472–11477.
25. Becker, P.B. and Horz, W. (2002) ATP-dependent nucleosome remodeling. *Annu. Rev. Biochem.*, **71**, 247–273.
26. Eberharter, A. and Becker, P.B. (2004) ATP-dependent nucleosome remodelling: factors and functions. *J. Cell Sci.*, **117**, 3707–3711.
27. Lusser, A. and Kadonaga, J.T. (2003) Chromatin remodeling by ATP-dependent molecular machines. *Bioessays*, **25**, 1192–1200.
28. Narlikar, G.J., Fan, H.Y. and Kingston, R.E. (2002) Cooperation between complexes that regulate chromatin structure and transcription. *Cell*, **108**, 475–487.
29. Smith, C.L. and Peterson, C.L. (2005) ATP-dependent chromatin remodeling. *Curr. Top. Dev. Biol.*, **65**, 115–148.
30. Srinivasan, S., Dorighi, K.M. and Tamkun, J.W. (2008) *Drosophila Kismet* regulates histone H3 lysine 27 methylation and early elongation by RNA polymerase II. *PLoS Genet.*, **4**, e1000217.
31. Takada, I., Mihara, M., Suzawa, M., Ohtake, F., Kobayashi, S., Igarashi, M., Youn, M.Y., Takeyama, K., Nakamura, T., Mezaki, Y. *et al.* (2007) A histone lysine methyltransferase activated by non-canonical Wnt signalling suppresses PPAR-gamma transactivation. *Nat. Cell Biol.*, **9**, 1273–1285.
32. Kim, H.G., Kurth, I., Lan, F., Meliciani, I., Wenzel, W., Eom, S.H., Kang, G.B., Rosenberger, G., Tekin, M., Ozata, M. *et al.* (2008) Mutations in CHD7, encoding a chromatin-remodeling protein, cause idiopathic hypogonadotropic hypogonadism and Kallmann syndrome. *Am. J. Hum. Genet.*, **83**, 511–519.
33. Murdoch, B. and Roskams, A.J. (2007) Olfactory epithelium progenitors: insights from transgenic mice and *in vitro* biology. *J. Mol. Histol.*, **38**, 581–599.
34. Monti-Graziadei, G.A., Margolis, F.L., Harding, J.W. and Graziadei, P.P. (1977) Immunocytochemistry of the olfactory marker protein. *J. Histochem. Cytochem.*, **25**, 1311–1316.
35. Saito, H., Kubota, M., Roberts, R.W., Chi, Q. and Matsunami, H. (2004) RTP family members induce functional expression of mammalian odorant receptors. *Cell*, **119**, 679–691.
36. Nadi, N.S., Head, R., Grillo, M., Hempstead, J., Grannot-Reisfeld, N. and Margolis, F.L. (1981) Chemical deafferentation of the olfactory bulb: plasticity of the levels of tyrosine hydroxylase, dopamine and norepinephrine. *Brain Res.*, **213**, 365–377.
37. Hegg, C.C. and Lucero, M.T. (2004) Dopamine reduces odor- and elevated-K(+)-induced calcium responses in mouse olfactory receptor neurons *in situ*. *J. Neurophysiol.*, **91**, 1492–1499.
38. Banger, K.K., Foster, J.R., Lock, E.A. and Reed, C.J. (1994) Immunohistochemical localisation of six glutathione *S*-transferases within the nasal cavity of the rat. *Arch. Toxicol.*, **69**, 91–98.

39. Krishna, N.S., Getchell, T.V. and Getchell, M.L. (1994) Differential expression of alpha, mu and pi classes of glutathione *S*-transferases in chemosensory mucosae of rats during development. *Cell Tissue Res.*, **275**, 435–450.
40. McEwen, D.P., Koenekoop, R.K., Khanna, H., Jenkins, P.M., Lopez, I., Swaroop, A. and Martens, J.R. (2007) Hypomorphic CEP290/NPHP6 mutations result in anosmia caused by the selective loss of G proteins in cilia of olfactory sensory neurons. *Proc. Natl Acad. Sci. USA*, **104**, 15917–15922.
41. Fath, M.A., Mullins, R.F., Searby, C., Nishimura, D.Y., Wei, J., Rahmouni, K., Davis, R.E., Tayeh, M.K., Andrews, M., Yang, B. *et al.* (2005) Mkks-null mice have a phenotype resembling Bardet-Biedl syndrome. *Hum. Mol. Genet.*, **14**, 1109–1118.
42. Kulaga, H.M., Leitch, C.C., Eichers, E.R., Badano, J.L., Lesemann, A., Hoskins, B.E., Lupski, J.R., Beales, P.L., Reed, R.R. and Katsanis, N. (2004) Loss of BBS proteins causes anosmia in humans and defects in olfactory cilia structure and function in the mouse. *Nat. Genet.*, **36**, 994–998.
43. Reed, R.R. (1992) Signaling pathways in odorant detection. *Neuron*, **8**, 205–209.
44. Calof, A.L., Bonnin, A., Crocker, C., Kawauchi, S., Murray, R.C., Shou, J. and Wu, H.H. (2002) Progenitor cells of the olfactory receptor neuron lineage. *Microsc. Res. Tech.*, **58**, 176–188.
45. Calof, A.L., Mumm, J.S., Rim, P.C. and Shou, J. (1998) The neuronal stem cell of the olfactory epithelium. *J. Neurobiol.*, **36**, 190–205.
46. Calof, A.L., Rim, P.C., Askins, K.J., Mumm, J.S., Gordon, M.K., Iannuzzelli, P. and Shou, J. (1998) Factors regulating neurogenesis and programmed cell death in mouse olfactory epithelium. *Ann. N. Y. Acad. Sci.*, **855**, 226–229.
47. Iwai, N., Zhou, Z., Roop, D.R. and Behringer, R.R. (2008) Horizontal basal cells are multipotent progenitors in normal and injured adult olfactory epithelium. *Stem Cells*, **26**, 1298–1306.
48. Nicolay, D.J., Doucette, J.R. and Nazarali, A.J. (2006) Transcriptional regulation of neurogenesis in the olfactory epithelium. *Cell. Mol. Neurobiol.*, **26**, 803–821.
49. Weiler, E. and Farbman, A.I. (1997) Proliferation in the rat olfactory epithelium: age-dependent changes. *J. Neurosci.*, **17**, 3610–3622.
50. Bagchi, A., Papazoglu, C., Wu, Y., Capurso, D., Brodt, M., Francis, D., Bredel, M., Vogel, H. and Mills, A.A. (2007) CHD5 is a tumor suppressor at human 1p36. *Cell*, **128**, 459–475.
51. Goehler, H., Lalowski, M., Stelzl, U., Waelter, S., Stroedicke, M., Worm, U., Droege, A., Lindenberg, K.S., Knoblich, M., Haenig, C. *et al.* (2004) A protein interaction network links GIT1, an enhancer of huntingtin aggregation, to Huntington's disease. *Mol. Cell*, **15**, 853–865.
52. Minty, A., Dumont, X., Kaghad, M. and Caput, D. (2000) Covalent modification of p73alpha by SUMO-1. Two-hybrid screening with p73 identifies novel SUMO-1-interacting proteins and a SUMO-1 interaction motif. *J. Biol. Chem.*, **275**, 36316–36323.
53. Schmidt, D.R. and Schreiber, S.L. (1999) Molecular association between ATR and two components of the nucleosome remodeling and deacetylating complex, HDAC2 and CHD4. *Biochemistry*, **38**, 14711–14717.
54. Stelzl, U., Worm, U., Lalowski, M., Haenig, C., Brembeck, F.H., Goehler, H., Stroedicke, M., Zenkner, M., Schoenherr, A., Koeppen, S. *et al.* (2005) A human protein–protein interaction network: a resource for annotating the proteome. *Cell*, **122**, 957–968.
55. Tai, H.H., Geisterfer, M., Bell, J.C., Moniwa, M., Davie, J.R., Boucher, L. and McBurney, M.W. (2003) CHD1 associates with NCoR and histone deacetylase as well as with RNA splicing proteins. *Biochem. Biophys. Res. Commun.*, **308**, 170–176.
56. Tong, J.K., Hassig, C.A., Schnitzler, G.R., Kingston, R.E. and Schreiber, S.L. (1998) Chromatin deacetylation by an ATP-dependent nucleosome remodelling complex. *Nature*, **395**, 917–921.
57. Jepsen, K., Solum, D., Zhou, T., McEvilly, R.J., Kim, H.J., Glass, C.K., Hermanson, O. and Rosenfeld, M.G. (2007) SMRT-mediated repression of an H3K27 demethylase in progression from neural stem cell to neuron. *Nature*, **450**, 415–419.
58. Lunyak, V.V., Burgess, R., Prefontaine, G.G., Nelson, C., Sze, S.H., Chenoweth, J., Schwartz, P., Pevzner, P.A., Glass, C., Mandel, G. *et al.* (2002) Corepressor-dependent silencing of chromosomal regions encoding neuronal genes. *Science*, **298**, 1747–1752.
59. Schnetz, M.P., Bartels, C.F., Shastri, K., Balasubramanian, D., Zentner, G., Balaji, R., Zhang, X., Song, L., Wang, Z., LaFramboise, T., Crawford, G.E. and Scacheri, P.C. (2009) Genomic distribution of CHD7 on chromatin tracks H3K4 methylation patterns. *Genome Res.*, February 27 [Epub ahead of print].
60. Omodei, D., Acampora, D., Mancuso, P., Prakash, N., Di Giovannantonio, L.G., Wurst, W. and Simeone, A. (2008) Anterior–posterior graded response to Otx2 controls proliferation and differentiation of dopaminergic progenitors in the ventral mesencephalon. *Development*, **135**, 3459–3470.
61. Shou, J., Murray, R.C., Rim, P.C. and Calof, A.L. (2000) Opposing effects of bone morphogenetic proteins on neuron production and survival in the olfactory receptor neuron lineage. *Development*, **127**, 5403–5413.
62. Shou, J., Rim, P.C. and Calof, A.L. (1999) BMPs inhibit neurogenesis by a mechanism involving degradation of a transcription factor. *Nat. Neurosci.*, **2**, 339–345.
63. Jongmans, M.C., van Ravenswaaij-Arts, C.M., Pitteloud, N., Ogata, T., Sato, N., Claahsen-van der Grinten, H.L., van der Donk, K., Seminara, S., Bergman, J.E., Brunner, H.G. *et al.* (2009) CHD7 mutations in patients initially diagnosed with Kallmann syndrome—the clinical overlap with CHARGE syndrome. *Clin. Genet.*, **75**, 65–71.
64. Doty, R.L. (1997) Studies of human olfaction from the University of Pennsylvania Smell and Taste Center. *Chem. Senses*, **22**, 565–586.
65. Double, K.L., Rowe, D.B., Hayes, M., Chan, D.K., Blackie, J., Corbett, A., Joffe, R., Fung, V.S., Morris, J. and Halliday, G.M. (2003) Identifying the pattern of olfactory deficits in Parkinson disease using the Brief Smell Identification Test. *Arch. Neurol.*, **60**, 545–549.
66. Kjelvik, G., Sando, S.B., Aasly, J., Engedal, K.A. and White, L.R. (2007) Use of the Brief Smell Identification Test for olfactory deficit in a Norwegian population with Alzheimer's disease. *Int. J. Geriatr. Psychiatry*, **22**, 1020–1024.
67. Salerno-Kennedy, R., Cusack, S. and Cashman, K.D. (2005) Olfactory function in people with genetic risk of dementia. *Ir. J. Med. Sci.*, **174**, 46–50.
68. Sclafani, A.M., Skidmore, J.M., Ramaprakash, H., Trumpp, A., Gage, P.J. and Martin, D.M. (2006) Nestin-Cre mediated deletion of Pitx2 in the mouse. *Genesis*, **44**, 336–344.
69. Osborne, M.P. and Comis, S.D. (1991) Preparation of inner ear sensory hair bundles for high resolution scanning electron microscopy. *Scanning Microsc.*, **5**, 555–564.
70. Anderson, D.W., Probst, F.J., Belyantseva, I.A., Fridell, R.A., Beyer, L., Martin, D.M., Wu, D., Kachar, B., Friedman, T.B., Raphael, Y. *et al.* (2000) The motor and tail regions of myosin XV are critical for normal structure and function of auditory and vestibular hair cells. *Hum. Mol. Genet.*, **9**, 1729–1738.
71. Beyer, L.A., Odeh, H., Probst, F.J., Lambert, E.H., Dolan, D.F., Camper, S.A., Kohrman, D.C. and Raphael, Y. (2000) Hair cells in the inner ear of the pirouette and shaker 2 mutant mice. *J. Neurocytol.*, **29**, 227–240.
72. Raphael, Y., Kobayashi, K.N., Dootz, G.A., Beyer, L.A., Dolan, D.F. and Burmeister, M. (2001) Severe vestibular and auditory impairment in three alleles of Ames waltzer (av) mice. *Hear. Res.*, **151**, 237–249.
73. Washburn, K.B., Turner, T.J. and Talamo, B.R. (2002) Comparison of mechanical agitation and calcium shock methods for preparation of a membrane fraction enriched in olfactory cilia. *Chem. Senses*, **27**, 635–642.